

Integrated geophysical and geochemical study for investigating the hydrocarbon potentiality of West Dakhla area, Western Desert, Egypt, as an extension of Libyan Kufra basin

Ashraf GHONEIMI¹ , Nashat S. GAWISH², Muhammad NABIH^{1,*} 

¹ Zagazig University, Faculty of Science, Geology Department, 44519, Zagazig, Egypt;
e-mails: aeghoneimy@science.zu.edu.eg, mnabih@science.zu.edu.eg

² Former chief geophysicist, Dana Petroleum Company, Egypt;
e-mail: nashat_gawish_2@yahoo.com

Abstract: The present study represents an integrated study using the potential field maps and well geochemical data of the West Dakhla area in the western central area of the Western Desert area, Egypt. The potential field data are represented by the airborne gravity and total magnetic maps acquired by the Nuclear Material Authority (NMA), Egypt, on behalf of Dana Petroleum Company. The geochemical data consist of geochemical analysis in Ammonite-1 well that were done for source rock evaluation. Different processing techniques on the gravity and magnetic maps are carried out for separating the regional and residual separation and filtering. Modelling and Euler deconvolution tools are utilized for proposing the depth to basement and constructing basement-depth maps to infer the basin configuration of the study area. Before acquiring the present geophysical data, the study area wasn't subjected to any exploration investigations. Therefore, these data and this study are considered as the first efforts carried out and submitted for publication in this area. In addition, a comparison of the present basin is done with matched basins in southern Libya, where this basin is expected to have similar geological features. The study indicates that the studied basin may be a part of a wider basin extending in Egypt and Libya. This basin is expected to have the thickness and features that are favourable for hydrocarbon habitat. The geochemical analysis shows TOC values ranging from poor to very good source rock potentiality.

Key words: West Dakhla area, Sahara Desert, Kufra basin, geochemical analysis, Ammonite-1 well, potential geophysics

1. Introduction

The northern part of the Western Desert (WD) was the destination for many of the operating companies in Egypt. However, there is growing interest in

*corresponding author, e-mail: mnabih@science.zu.edu.eg

many other parts of WD, and the interest may extend to the West and south West where West Dakhla study area is located. The broad view of the regional free-air gravity anomaly map derived from Sandwell satellite (*Sandwell and Smith, 2009; Sandwell et al, 2013, 2014*) of the southwestern part of Egypt and the south-eastern part of our neighbour Libya (Fig. 1), where the prolific Kufra basin is located, gives impression that West Dakhla related basins and/or troughs may be an extent of Kufra basin at its north-eastern part through some parts of the uplifted areas. The West Dakhla area is located at the Western part of the WD (longitudes $15^{\circ} 00'$ and $16^{\circ} 30'$ E and latitudes $25^{\circ} 15'$ and $26^{\circ} 30'$ N) (Fig. 1). The study aims to show the contribution of potential (gravity and magnetic) data in delineating the structural framework and thickness of the basin/basins in the study area. This is achieved by enhancement and interpretation of gravity and magnetic maps. The interpretation will be integrated with the available well, seismic and geologic data.

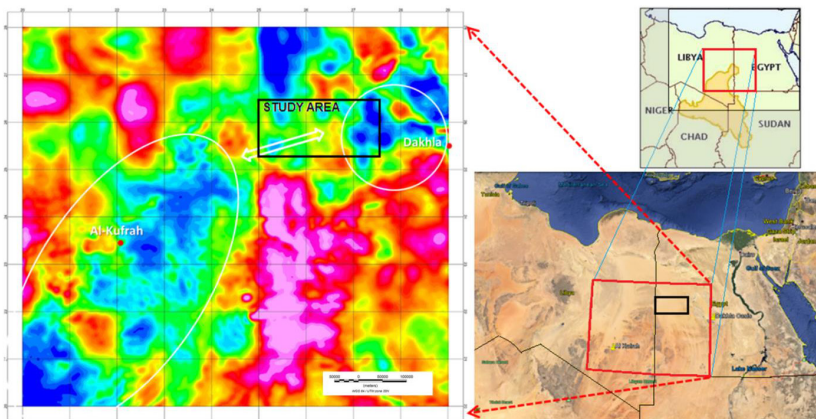


Fig. 1. The regional Sandwell satellite-derived gravity map of the Libyan portion of Kufra basin relative to the Egyptian southwestern part of the Western Desert. Study area is shown as black rectangle.

2. Geological setting

The study area slopes gently from south to north, topographically. Except for the valley that runs to the east and northeast of the central eastern portion of the area, no topographical features are evident. The surface of

the study area is mainly covered by sand dunes trending from Quaternary, N–S. Paleocene and undivided Cretaceous rocks are exposed in the eastern portion and southwestern corner.

2.1. Major structural framework in Sahara Desert

Figure 2 illustrates the structural framework of the Eastern Sahara. The wide area basins are created by the contribution of the vertical epirogenic movements, divided by slight uplift or subsidence zones. The central Sahara consists of normal fairly trends of structural development, a younger one with an orientation of about NE and an older NNW-striking pattern (*Klitzsch, 1984, 1990, 2000; Klitzsch and Squyres, 1990; Gossel et al., 2004;*

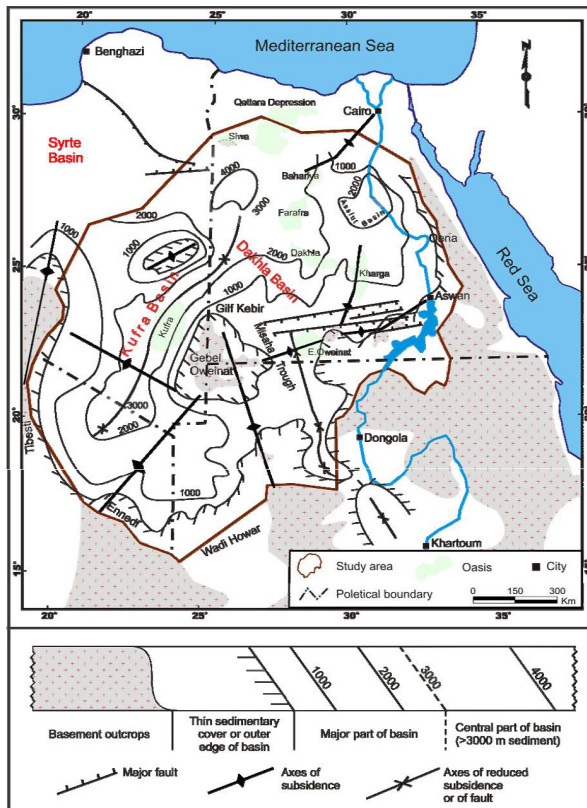


Fig. 2. General structural framework of the NASA, (adapted from *Klitzsch, 1984*).

Schmieder et al., 2009; Salama and El Ebaidi, 2016; Hallett and Clark-Lowes, 2016; Hamimi et al., 2020).

The Oweinat-Howar Uplift (early Paleozoic) spreads through Gebel Oweinat (in southwestern Egypt) to the eastern part of Wadi Howar (in Sudan). This area is divided by this uplift into the Dakhla basin in the southwest Egypt and the comparatively small, minor basins which parallel to the Howar-Oweinat Uplift in the Kufra basin (*Meshref, 1990*). The dip of the continental sediments (Paleozoic and Mesozoic) in Kufra basin follows the shape of the edges of the basin (*Bellini and Massa, 1980*). The tectonic map of the basement illustrates the major ENE–WSW direction faults crossing northern Egypt (*Schlumberger, 1995*), with non-prospective ridges were formed by the up-thrown blocks and petroleum basins were formed by the broad down-dropped blocks in the WD. The Wide sedimentary basins and ridges were formed during the Cretaceous by the lateral movements that occurred along the faults and created small and large parallel faults. The anticlinal structure traps that hold the hydrocarbon accumulations were created along these faults. These anticlines are subdivided into separate reservoir blocks by even smaller faults and can cut blocks into distinct reservoir compartments. The basement of Egypt was made of several different studies. A good picture of the foundations can contribute to a better understanding of the sediments on top of these structures (courtesy of Dr. Wafik Meshref, EGPC) (*Schlumberger, 1995*).

The stable shelf is an area with ill-defined borders that is characterized by a relatively shallow basement (Precambrian) underlying continental and epicontinental sedimentary rocks (*Said, 1962*). In the ‘stable shelf’ south of the Bahariya Oasis, gravity, magnetic, and seismic surveys, and a few boreholes drilled during the 1980s and 1990s, revealed the rift basins of Mesozoic Era such as El Misaha, Nuqura, Asyut and Dakhla (*Taha, 1992; Moustafa et al., 2003; Farooqui et al., 2012*).

During the Phanerozoic Eon in the WD, can be recognized the following six major geotectonic phases; Caledonian Cycle during Cambrian-Devonian Period, Variscan-Hercynian (Late Paleozoic), Cimmerian/Tethyan belongs to Triassic-Early Cretaceous, the Sub-Hercynian-Early of Syrian Arc (Turonian-Santonian), the main phase of Syrian Arc (Paleogene) and as more extensive information has been obtained through geological and geophysical studies, the Red Sea period (Oligocene Miocene) has changed in places.

Time depends on Said's terminology for the structural regime; the so-called Stable Shelf, for example, can only be perceived as a stable Mesozoic field.

The Stable Shelf, consisting of large north-south oriented Caledonian highs and lows intersected by the old Paleozoic system's subsidiary Early Hercynian east-west faults, is replaced to the north by the Unstable Shelf, where NW–SE and NE–SW oriented features that disrupt the Mesozoic portion overprint the older Paleozoic/Nubian patterns. The break-up of the geotectonic plate and subsequent intraplate movements provide an overall basis for understanding the formation of NE Africa and hence the Western Desert (EGPC, 1992).

2.2. Stratigraphy and sedimentation

The borders between the Western and Eastern Sahara of the Libyan Desert are situated along the sequence of highlands including the mountains of Erdis, Tibesti, Ennedi, and Fezzan region of Hamada (in Libya) and the NW of El-Fashir (in Sudan). This desert's eastern side is confined to the Nile Valley. The mountainous areas of Darfur and Kordofan in Sudan are separated from the southern margins, while the desert stretches northwards until it meets the Mediterranean coastline (Fig. 3).

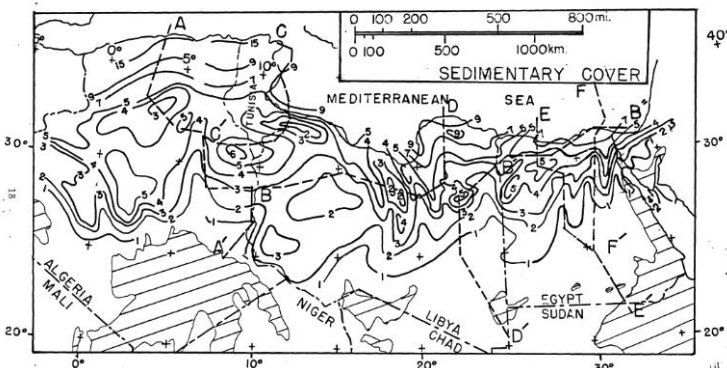


Fig. 3. Approximate thickness in thousands of meters, partly restored where erosion has taken place, sedimentary cover, north-central and northeastern Africa. Compiled from numerous sources (Peterson, 1985).

The basement complex rocks are progressively overlaid by a sequence of un-fossiliferous Nubian Sandstone Series deposits consisting of sandstones, sands, shales, and clays. The thickness of the Nubian Sandstone Sequence

ranges from approximately 1800 m at the Bahariya oasis, and 900 m in the northern locations of Kharga oasis. The thickness of the Nubian Sandstone reaches of more than 3500 meters in the northern parts of the Dakhla basin and more than 4500 m in the north-western locations of the Kufra basin (Sefelnasr, 2007). The similarity of stratigraphic position and thick sedimentary column sedimentation could be demonstrated at several locations in the Sahara region (Libya and Egypt) (Figs. 4 and 5).

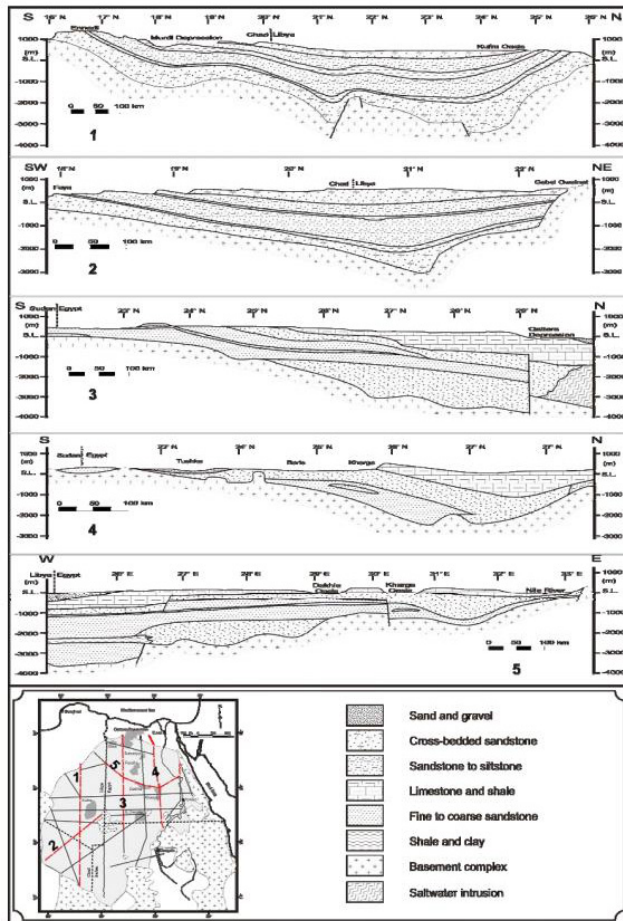


Fig. 4. Lithostratigraphic sections of the NSAS, profile locations are plotted in the lower index map (compiled from Hissene, 1986; Kheir, 1986; Hesse et al., 1987; Sefelnasr, 2007).

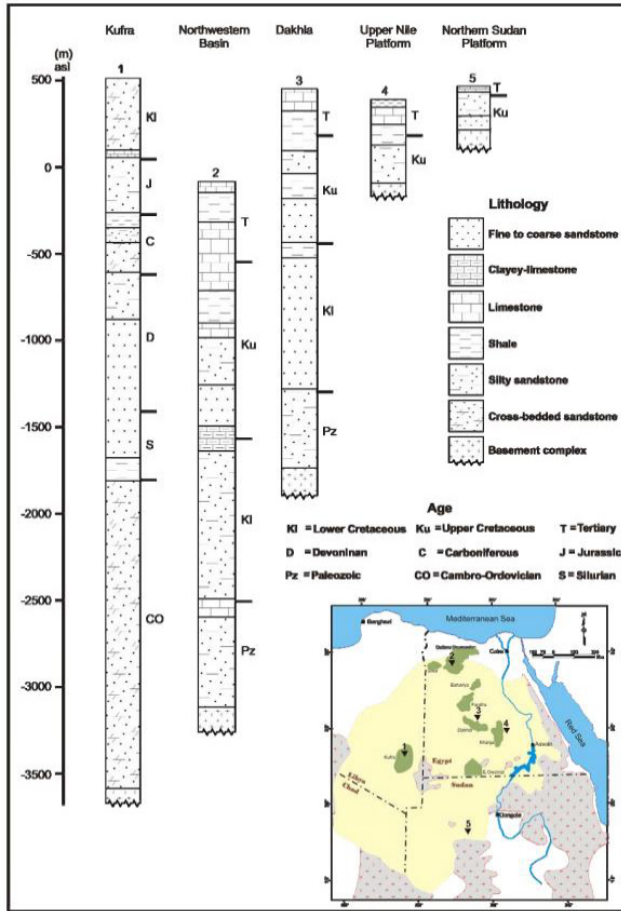


Fig. 5. Columnar sections for locations within the NASA (adapted from Thorweihe and Heini, 2002; Sefelnasr, 2007).

3. Petroleum habitat

3.1. Petroleum habitat in Egypt

There are several hydrocarbon basins in the WD in Egypt and are characterized by a Paleozoic segment thickening southwest ward and Mesozoic and Tertiary strata thickening northward prism, disrupted by the Sharib-Sheiba high major east-west trend. As a result of the Hercynian Orogeny, this re-

gional ridge was formed (*EGPC, 1992*). The Western Desert has the main hydrocarbon system elements (source, reservoir, seal and traps) that support the existence of hydrocarbon accumulations (*EGPC, 1992; Moustafa et al., 2003; Farooqui et al., 2012; Abrams et al., 2016; Afife et al., 2017; El Sherief et al., 2020; Cheng, 2020*) (Figs. 6 and 7).

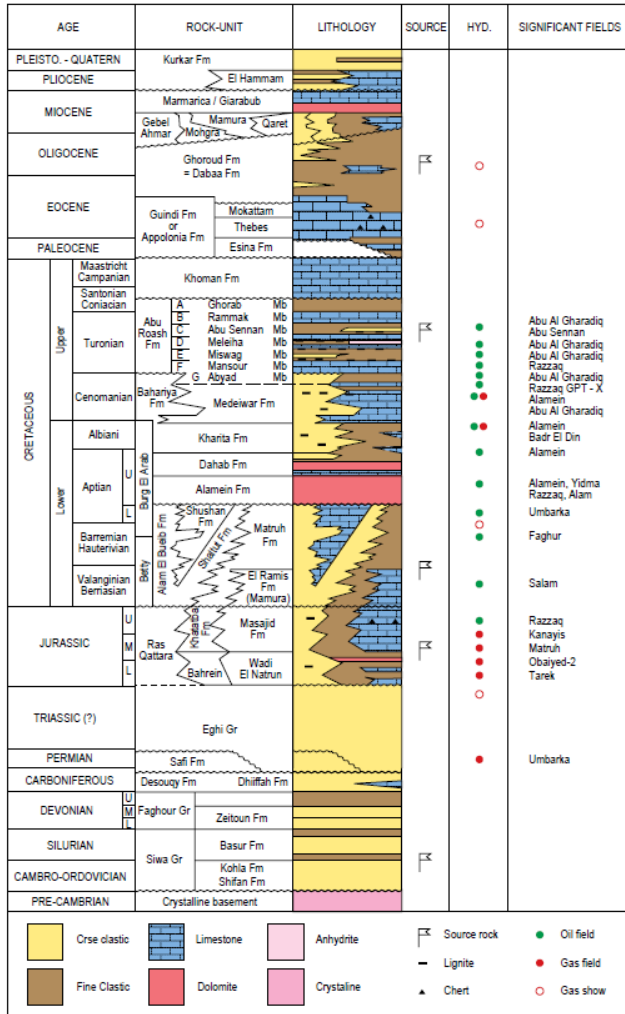


Fig. 6. Generalize stratigraphic column of Western Desert, Egypt (*Schlumberger 1984; 1995*).

sediments overlying basement rocks (Fig. 8). The Paleozoic sedimentary portion of up to 8350 m thick consists mainly of marine deposits located in the sedimentary basins and sub-basins of North Africa (Lüning *et al.*, 1999; Hallett and Clark-Lowes, 2016). The existing geometry of Kufra basin tends to be mainly resulted due to the tectonics of the Hercynian age. Due to the shortage of seismic data, the subsurface geology is unidentified and the stratigraphy is poorly understood. Fortunately, there are several economically relevant horizons including the source rocks of Tanzuft Shale can be examined in more detail in surface exposures (Meinhold *et al.*, 2013; Meinhold *et al.*, 2015).

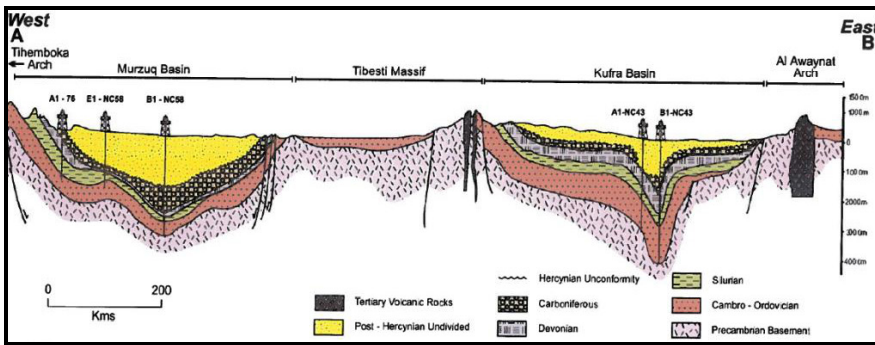


Fig. 8. Geological cross-section through Murzuq and Kufra basins (Bellini and Massa, 1980; Lüning *et al.*, 2000).

There are no significant discoveries to date in the Kufra basin, but expectations remain high. The Kufra basin in Libya has seen an interested in by many American companies. The Kufra basin has great similarities, including tectonic history and stratigraphic nomenclature, with the Muruzq basin. In Kufra basin, the Mamuniyat Formation (Upper Ordovician) sandstone and the Tanzuft Shale (Lower Silurian) may represent the best possible petroleum system. In North Africa, the petroleum geology of Neo-Proterozoic to Early Cambrian (Infra-Cambrian) is beginning nowadays to be known, particularly after the occurrence of confirmed plays in Mauritania (Klitzsch, 2000).

Lüning *et al.* (1999) indicated that black shales or organic-rich limestones have both the Infra-Cambrian graben and Infra-Cambrian sediments that are possible source rocks. He proposed that the Infra-Cambrian sediments

and Infra-Cambrian graben have organic-rich Limestones or black shales which represent potential source rock. This recommends the opportunity of the Infra-Cambrian play with fractured Limestones or the sandstones as reservoirs (Fig. 9). As mapped (Fig. 10), the maximum Paleozoic thickness is over 9000 feet. Thickening from the West Desert to the Siwa basin depocenter in Libya occurs south, west and northward (EGPC, 1992). This thickening is obscured by erosion that at the end of the Paleozoic created regional unconformities.

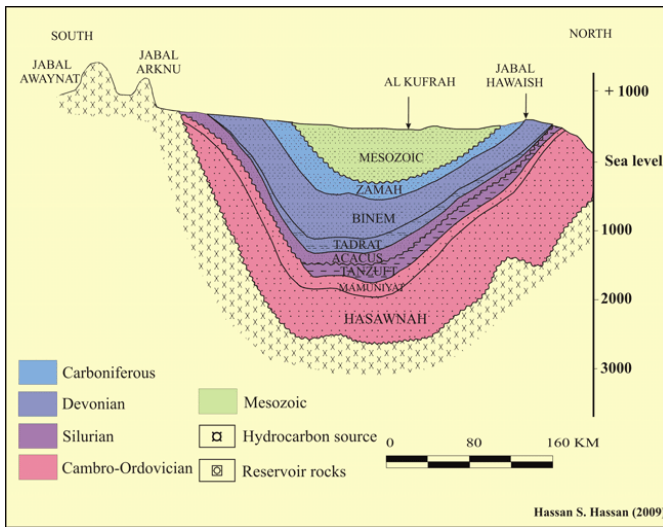


Fig. 9. N–S cross section through Kufra basin (modified after Pallas, 1980).

Although Siwa basin is a northeast continuation of the Kufra basin in Libya and similar to the Dakhla basin, there is not enough knowledge about the Dakhla basin; it thickens into the Kufra basin to the west. The Siwa basin is a Paleozoic epicontinental basin created as a consequence of Hercynian Orogeny by gentle crustal downwards and faulting, resulting in the uppermost Paleozoic portion erosion. According to both the structural setting and the stratigraphic sequences in Eastern Libya (Kufra basin) and the Western Desert (Fig. 11), the source rock of the Upper Cretaceous, Lower Cretaceous, Jurassic or Silurian ages can be found, depending on the Egyptian geological setting in the area under investigation and in the Silurian Age rocks, if the area belongs to the Kufra basin since the structural pattern

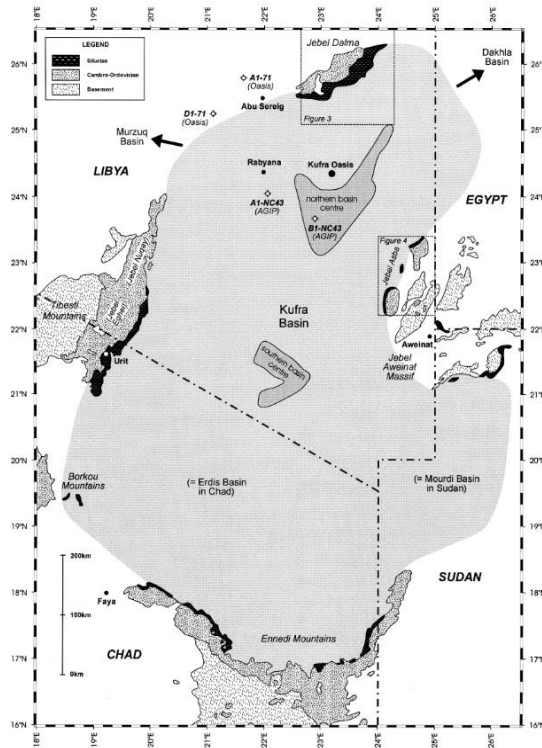


Fig. 10. Kufra basin and its outlining basement highs (Seber et al., 1997; IRC, 1985).

shown in the following figure assumed to be valid for the Western part of the western desert close to Kufra basin. The area under investigation may be similar to the Kufra basin.

4. Potential data interpretation

4.1. Source of data

The potential field data used in this study comprise two airborne gravity and total intensity magnetic maps (Figs. 12 and 13). The data have been acquired by the Nuclear Materials Authority (NMA) on behalf of Dana Petroleum Company at the 2014–2015 time periods. The data covers West Dakhla-1 and West Dakhla-2 Blocks, Western Desert, Egypt, with a total area of about 34480 km². The data are used in a grid of 500 m.

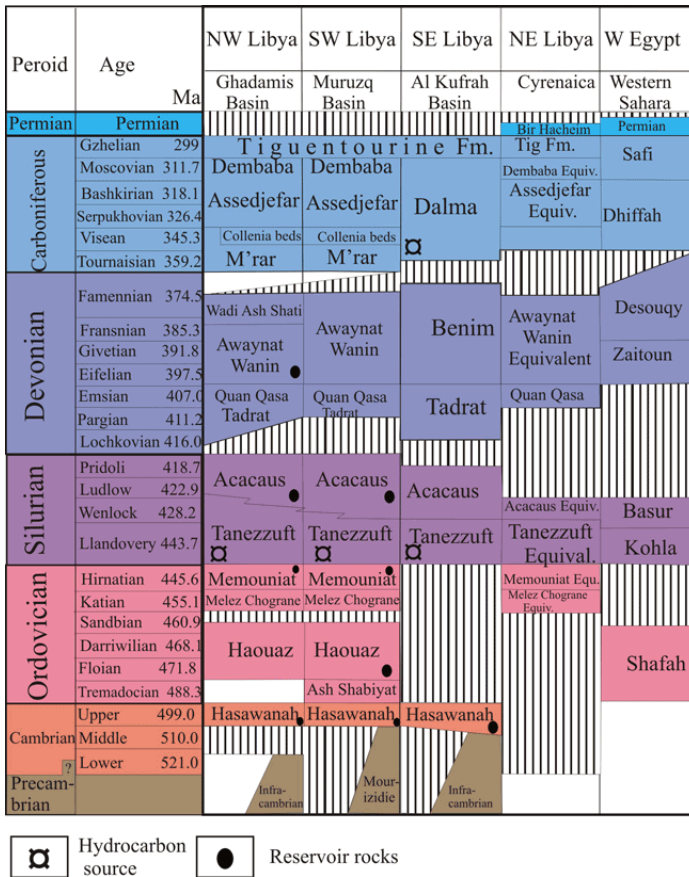


Fig. 11. Correlation chart between different basins in Libya, showing the stratigraphic Paleozoic section of basins in southern and eastern Libya and the distribution of reservoir and source rocks. <http://www.sepmstrata.org/page.aspx?pageid=1484>. Modified after Craig et al. (2008).

4.2. Methodology

The used airborne gravity and magnetic maps are investigated and integrated with other geophysical and geological maps to produce a structural picture for the investigated sedimentary basins and intersecting ridges of the area on the light of the probable petroleum systems. Several processing methods utilizing transformation and filtering techniques are used to correct and enhance the used data and to facilitate the interpretation purposes.

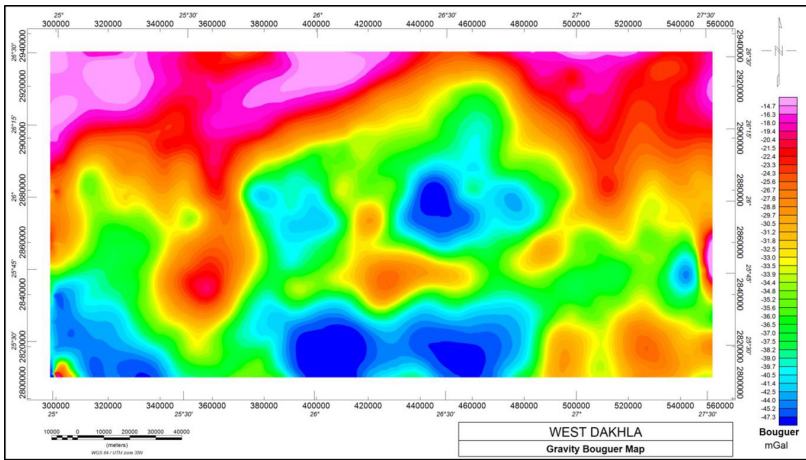


Fig. 12. Airborne Gravity Bouguer anomaly map.

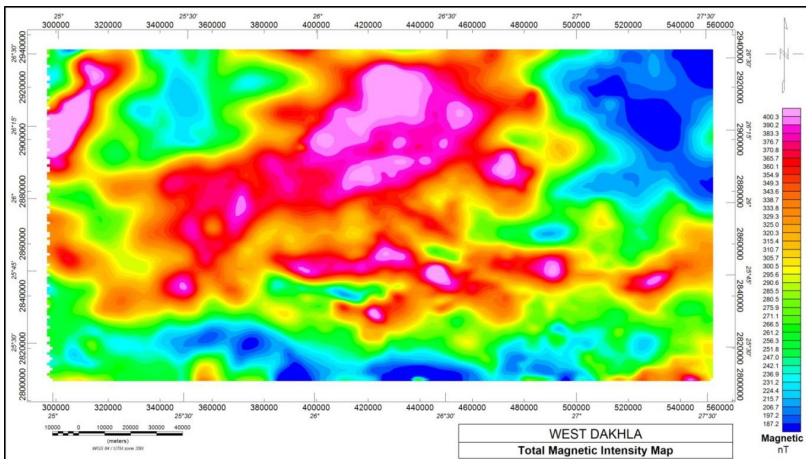


Fig. 13. Airborne total magnetic intensity (TMI) map.

4.3. Data processing and enhancement

The gravity and magnetic maps are analysed using transformations and enhancement techniques which are performed in the space and frequency domains. The Gaussian low- and high-pass filters and Butterworth low- and high-pass filters are executed to carry out the regional-residual sepa-

ration methods. Therefore, the regional and residual anomalies maps are constructed. Commonly, the residual maps, with increasing depth, indicate that, there are new negative anomalies, which are considered as downwardly continuing basins. Meanwhile, the positive anomalies could be regarded as promising sites for commercial accumulations in ridges. The residual RTP anomalies may reveal the great variation in the basement rocks mineralogical composition. The positive anomalies may be associated with basic types of basement rocks of high susceptibilities, while the negative ones may be accompanied with acidic basement rocks of low susceptibilities. On the other hand, the positive anomalies may be associated with uplifted blocks, horsts and/or elevated parts. The regional-residual separation methods are executed through applying different theoretical assumptions, both in the space domain and frequency domain using Gaussian and Butterworth low- and high-pass filters.

– Reduction to the Magnetic Pole (RTP)

The reduction to magnetic pole (RTP) process converts the total magnetic field from magnetic latitude, where the Earth's magnetic field is inclined, to a magnetic North pole, where the inducing field is vertical (inclination angle = 90). The shape of magnetic anomalies varies as a function of the geomagnetic latitudes. The reduction to the pole removes the effect of the inclination and declination of the Earth's magnetic field from the data. The resulting RTP magnetic field appears as it would be if the body was situated at the earth's magnetic pole, thus it simplifies the interpretation procedure.

The total magnetic intensity (TMI) map of the study area (Fig. 13) is reduced to pole (Fig. 14). Comparing the original TMI map with the RTP map, it is shown that there is a northern displacement in the positions of the resultant magnetic anomalies, because the RTP process removes the declination and inclination effect of the acquired magnetic measurement. In addition, the shapes of the anomalies are more centred above their causative sources. The investigation of the reduced to pole (RTP) magnetic map (Fig. 14) outlines a rapid change in the geological structural features and/or lithological composition of the subsurface. Correspondingly, different anomalies of varying amplitudes and frequencies are shown and reveal various causative sources, as well as varying compositions and depths.

– **Pseudo-Gravity Map**

The process of pseudo-gravity transformation is used in this study as a step to other depth estimation or edge-detection. The pseudo-gravity anomaly map (Fig. 15) is calculated using the reduction to the pole process followed by a vertical integration. This process is affected by the same uncertainties which are present in the calculation of the RTP field.

– **Butterworth Regional Filtering**

The Butterworth filter is applied as a low-pass filter on the RTP map in the frequency domain. The application of this filter is carried out utilizing different parameters in the Geosoft Oasis Montaj software. One of the advantages of applying the Butterworth filter is the ability to easily control the degree of the filter cut-off while fixing the central wave number. Figure 16 shows the regional map produced after applying Butterworth filter on the RTP map using 50 km wavelength cut-off. This map shows the regional anomalies the RTP map but with longer wavelength expressing the deeper geological structural sources.

– **Gaussian Regional Filtering**

The Gaussian regional filter is a smoothing filter that is applied on the used magnetic and gravity data as a low-pass filtering process. Figure 17 shows the regional map produced after applying both Butterworth and Gaussian filters on the RTP magnetic map with 50 km wavelength cut-off. The Gaussian regional filter is applied to obtain the regional component of the gravity map at the different spacings of 500, 1000 and 1500 m, respectively. These maps are largely similar, except a slightly more regional effect is increased with increasing the spacing. Figure 18 shows the regional gravity map at spacing 1500 m.

The low-pass wavelength filtering technique is applied on the gravity map with filter passes 50 (± 1000 m depth), 100 (± 2000 m depth), and 150 (± 3000 m depth), respectively. The regional gravity map obtained from these filters is largely similar, except a slightly more regional effect is increased with increasing the filter pass and structural depths. Figure 19 shows the regional gravity map at low-pass filter of 150 and depth of ± 3000 m depth. Faults are added to these maps as margins or edges of regional structures anomalies.

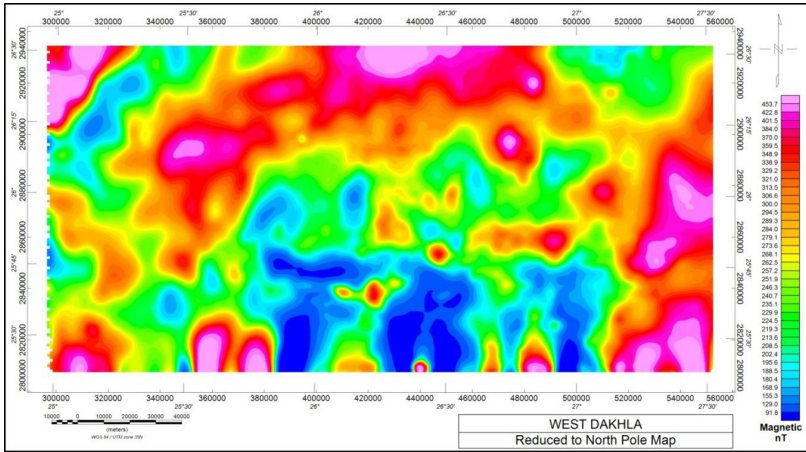


Fig. 14. Reduced to north pole magnetic (RTP) map.

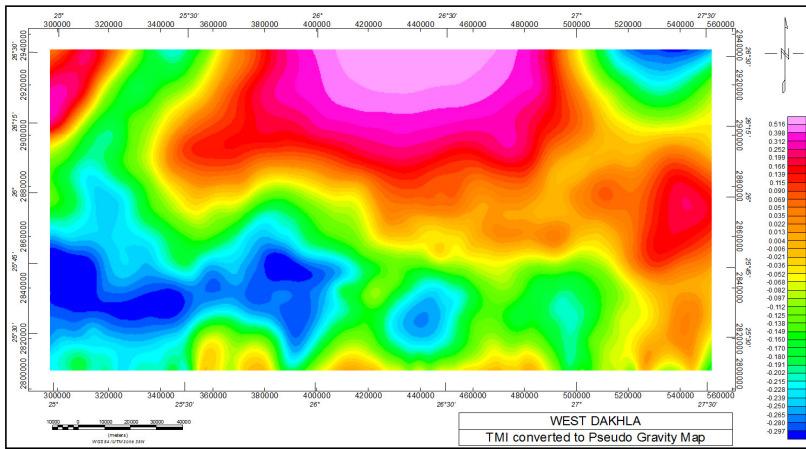


Fig. 15. Pseudo-gravity map applied on TMI map.

Residual maps are constructed from the gravity maps using the second derivative computed from the maximum gradient and residual separation at 500, 1000 and 1500 m spacing, respectively. These maps show the low-wavelength anomalies of local structures at shallower depths. The amplitude anomalies increase with decreasing the spacing and investigated structural features depths as shown in Fig. 20 which shows the residual component at 1500 m separation.

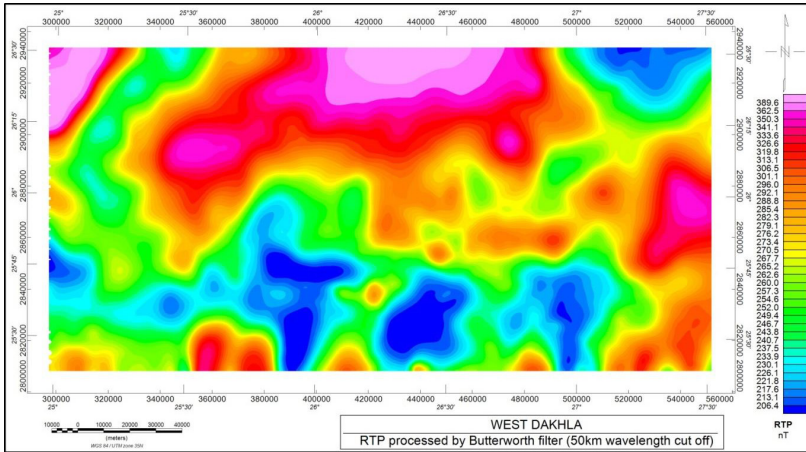


Fig. 16. RTP map filtered with Butterworth Low-Pass filter (50 km wavelength cut-off).

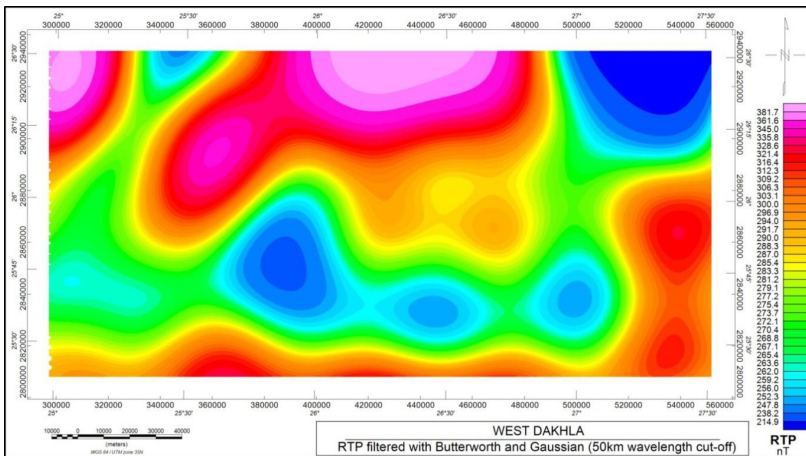


Fig. 17. RTP map filtered with Butterworth and Gaussian Low-Pass filters (50 km wavelength cut-off).

4.4. Data interpretation

The gravity and magnetic methods have a great deal in seeking anomalies caused by changes in the physical properties of subsurface rocks. Both methods have been in use for a long time, especially for reconnaissance sur-

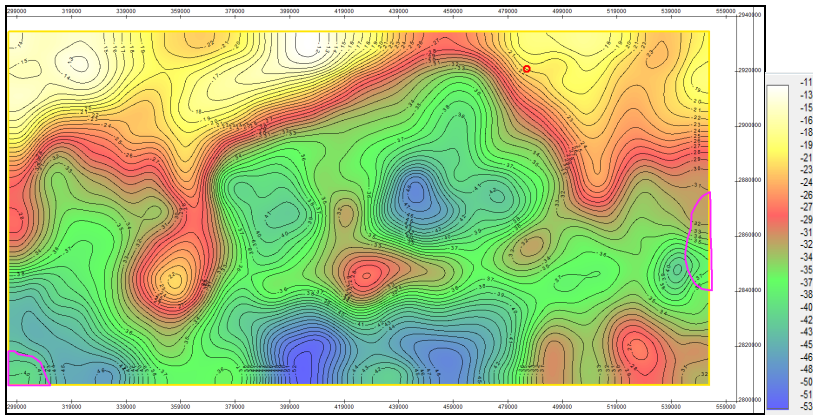


Fig. 18. Regional gravity anomaly map with 1500 m spacing (C.I. = 1 mGal).

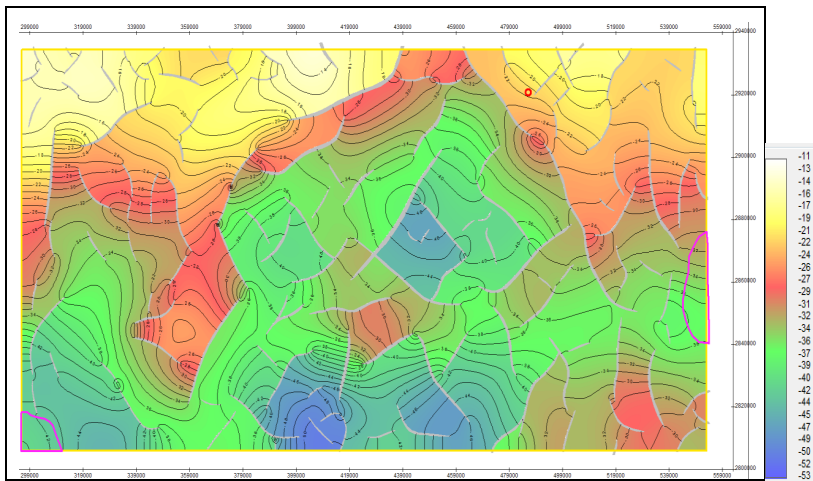


Fig. 19. Regional gravity anomaly map with filter pass 150 (± 3000 m depth) (C.I. = 1 mGal).

veys in the search for minerals and hydrocarbons. The objective of gravity data interpretation is to use the various characteristics (shape, amplitude, frequency and sharpness) of the gravity anomaly to infer the locations and structures which yield the gravity anomaly patterns shown in maps. This is carried out to describe several forms of geological structures of depths and sizes ranging from deep crustal to near-surface blocks. The magnetic data

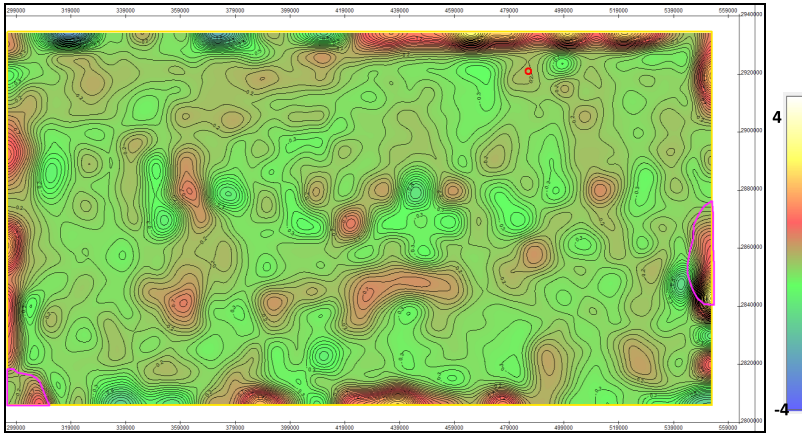


Fig. 20. Residual gravity anomaly map with 1500 m spacing (C.I. = 0.1 mGal).

is used to explore for oil to determine the depths to basement rocks and thus locate and define the extent of sedimentary basins.

4.5. 3D Euler deconvolution

The technique of 3D Euler deconvolution applies the Euler's homogeneity equation to gridded potential field data to identify the position, depth and nature of sources (*Reid et al., 1990*). Structure indices 0.0, 0.5 and 1.0 are routinely used for magnetic data. Since structural elements creating the basement blocks tend to have considerable lateral extent, $SI = 0$ tends to be indicative of deep the deep structure, whilst $SI = 0.5$, with more limited extent tend to be more characteristic of fault offsets in the overburden and therefore shallower features (Figs. 21 and 22). The Euler solution maps locate and outline the various causative sources all-over the area, including contacts, step-faults and dykes, as well as to estimate their depths and trends. These constrains are extremely linked with the structural systems and regional trend patterns in the underlying basement complex. It is shown that many variations in the basement depths lying in the range from about 3000 to 6000 m. All these structural elements of different trends and various depths may provide favourable conditions for hydrocarbon migration and preservation, in case of presence of source rocks; and encourages the geophysical exploration at the future times.

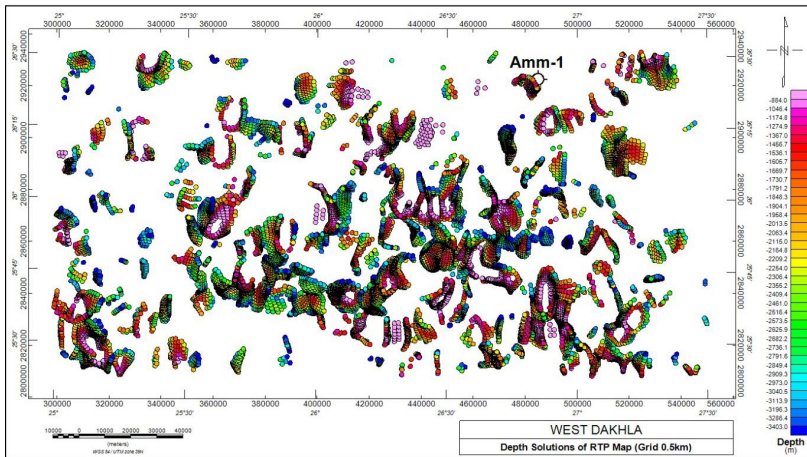


Fig. 21. Euler depth standard solutions at shallower contact depths (grid spacing 500 m).

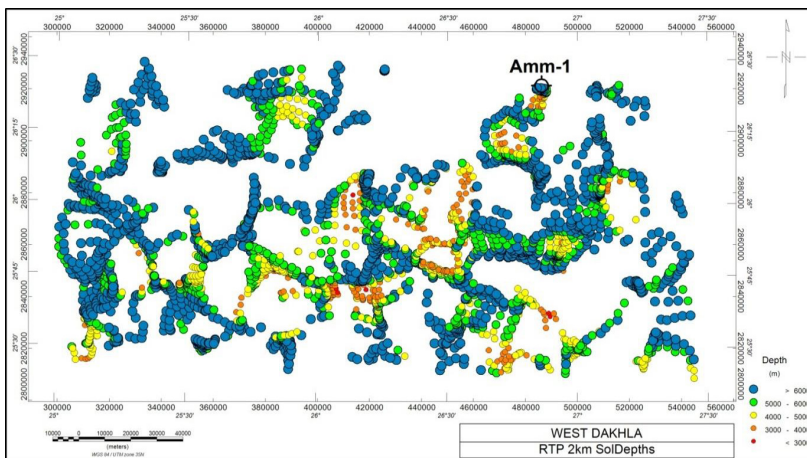


Fig. 22. Euler depth standard solutions at deeper contacts (grid spacing 2000 m).

4.6. Fault detection

The maximum gradient technique is applied to the gravity map to detect the contacts at the basement surface (Fig. 23). The absolute horizontal gradient of the magnetic RTP map is used to detect the contact pattern on the basement surface. These contact surfaces may represent fault planes or igneous intrusion surfaces.

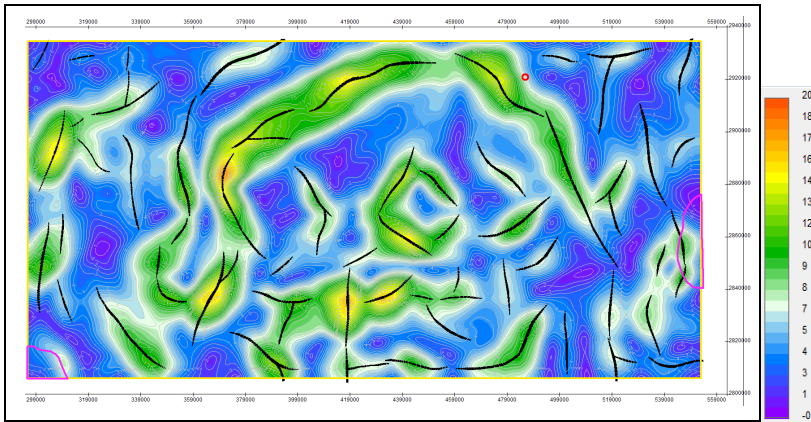


Fig. 23. The major geologic contacts from the maximum gradient at basement surface (C.I. = 0.5 (arbitrary unit)).

4.7. 2D forward modelling and depth estimation

The modelling technique is used in this study to create a geological model so that the calculated magnetic effect matches the observed gravity or magnetic anomaly profile. In the magnetic modelling process each separate polygon, that represents a structural or lithological feature, assigns a certain susceptibility value. The total effect of the magnetic bodies of individual polygons results in the magnetic anomaly through the processed profile.

The 2D magnetic interactive modelling is performed using the GM-SYS package of Geosoft Oasis Montaj software, integrated within Oasis Montaj (Northwest Geophysical Associates, NGA). Sixteen models (Fig. 24) are constructed in nearly two directions and distributed to pass through most major, moderate and minor anomalies, and to match some of the seismic sections occupying the northern sector of the area of study. Two models are shown for presentation in Fig. 25. These models are oriented N–S. One of these models (Fig. 26) passes through the Ammonite-1 well and overlaps the UER-20 seismic section. Matching the magnetic (RTP) model with the seismic section shows that the proposed basement top surface is not clear in the seismic section. This may be due to the lake of seismic data processing at this depth.

The depth values resulted from the 2D models are digitized and interpolated to construct the depth to basement map. The models and the depth

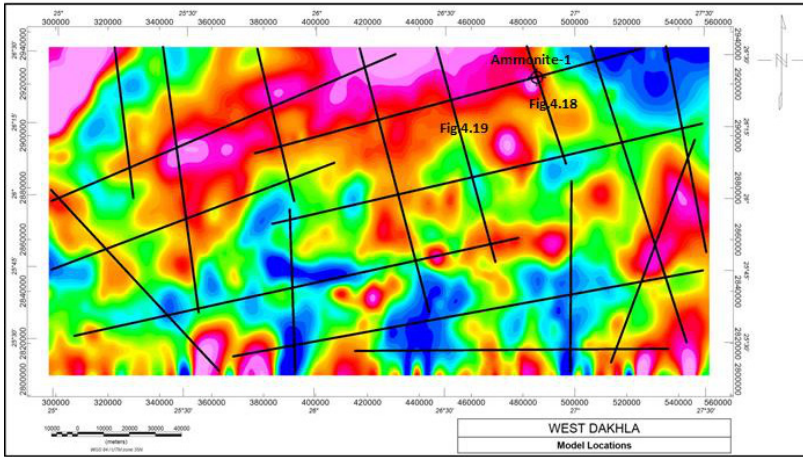


Fig. 24. Locations of profiles used for 2D RTP models.

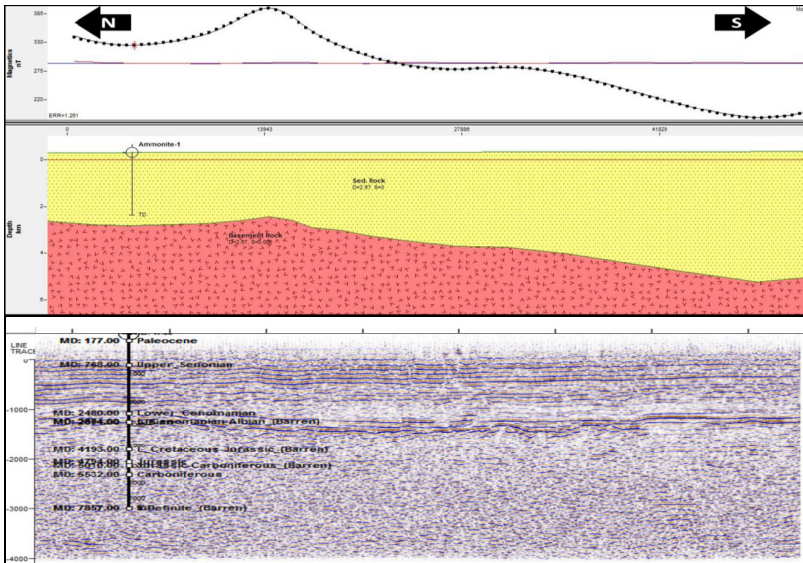


Fig. 25. 2D N-S RTP model passing through Ammonite-1 well and overlapping seismic section UER-20.

to basement map shows that the area is occupied mainly in the northern, south-eastern and north-western portions by three major highs, ranging in depth from about 2000 to 4000 m. On the other hand, the middle and

nearly southern portions are occupied by a major basin, ranging in depth between 4000 to 6000 m. This basin is dissected by high areas and subdivided into a number of sub-basins of different depth ranges. The major basin is partially closed and connected to the northeast to a deep basin which cover the north-eastern corner and may extend to out of the area. Another connection of the major basin is due to a linear depression in the north-western part of the study area. It is also shown that the main trend of both high and low areas is the northeast to southwest. Figure 27 shows the depth to basement maps based on gravity data.

5. Geochemical analysis

Geochemical analysis was performed to compare the type of kerogens in the area under investigation employing the Ammonite-1 well data with the kerogen types in the WD and the source rock of the Silurian age source rock (Fig. 28). The samples for the geochemical analysis from the Ammonite-1 well were taken down only to the carboniferous age and are characterized by Kerogen type III/II. The organic geochemical data of fifty-three shale samples were analysed section covers the interval from 18 m (Paleocene) to 1611 m (Carboniferous) in Ammonite-1 well. The geochemical data includes TOC, S1, S2, S3, Tmax, HI, OI and GP. The data were plotted divided into 8 groups based on age.

5.1. Organic matter richness (TOC wt%)

The TOC values recorded 0.05 wt% (at depth 450–456 m, 1486 ft) to 10.49 wt% (at depth 1266–1272 m, 4162 ft) with an average value of 0.74 wt% (Fig. 29-A) indicating a range varying between poor and very good source rock (*Peters, 1986*).

5.2. Hydrocarbon generation potential

To predict the source rock potentiality of the study area, the pyrolysis values of S1 and S2 of the formations are estimated and plotted. The S1 values are ranging from 0.09 to 8.86 mg/g rock with average value of 1.841 mg/g rock. The above-mentioned values of S1 in study area indicate a poor potential source rock for generation hydrocarbon (Fig. 29-B). The S2 values

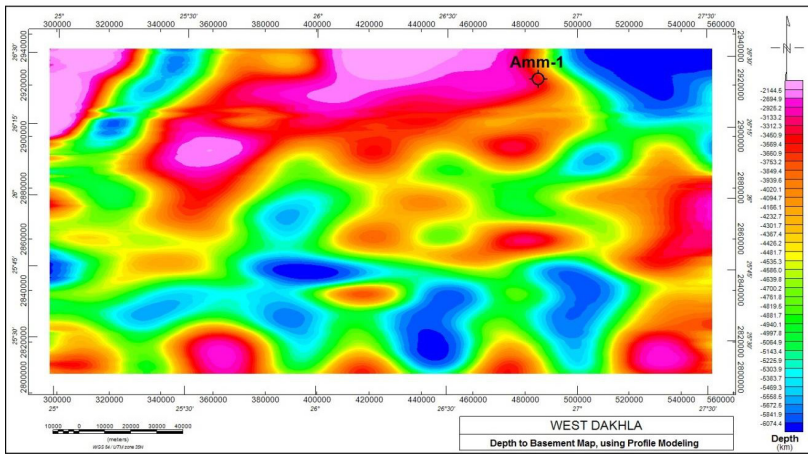


Fig. 26. Depth to basement based on 2D digitized models.

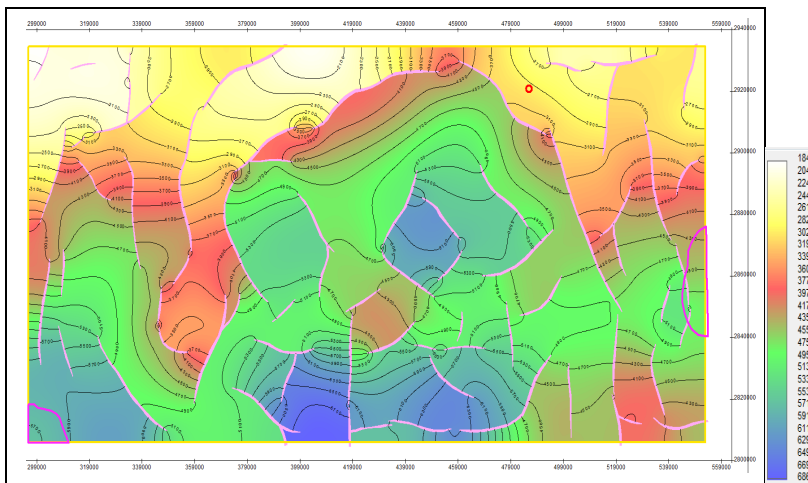


Fig. 27. Basement depth map with faults (C.I.= 200 m).

are ranging from 0.16 to 18.63 mg/g rock with average value 2.47 mg/g rock indicating poor to good generating range (Fig. 29-C). Poor genetic potential is indicated from the values along the section that is ranging from 0.29 to 20.17 mg/g rocks few are good at the Jurassic and L. Cretaceous-Jurassic Ages (Fig. 29-D).

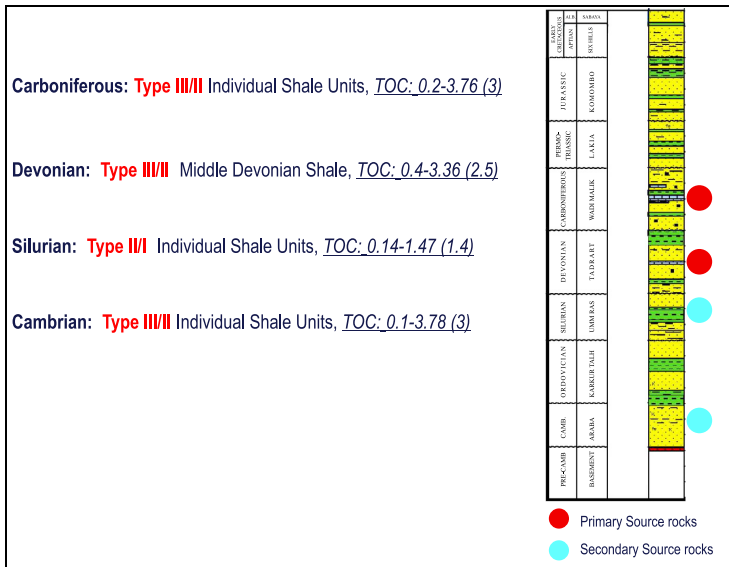


Fig. 28. General kerogen types in Western Desert.

5.3. Types of organic matter

As stated by *Hollander et al. (1991)*, to establish the full connectivity of the organic matter (OM) in a rock, the OM content must be enough. Therefore, the type and quantity of OM is estimated in this area by Rock-Eval Pyrolysis and kerogen isolates. Figure 30-A shows the relationship between HI and OI of kerogen samples and indicates type (III) kerogen (*Peters et al., 2016*). The HI values range from 22 to 324 mg/g with average of 114 mg/g (Fig. 30-B).

5.4. Maturation of organic matter

The maximum pyrolysis temperature (T_{max}) is defined as the maximum value of hydrocarbons released from kerogen cracking which occurs during pyrolysis (top of S2 peak). The value of T_{max} is an indication of the stage of the organic matter maturation. Therefore, the organic matter maturation is precisely estimated using the maximum pyrolysis temperature (T_{max}) value. The T_{max} values are ranging from 419°C (at depth 126–132 m, 423 ft) to 437C (at depth 1602–1605 m, 5259 ft) with an average value

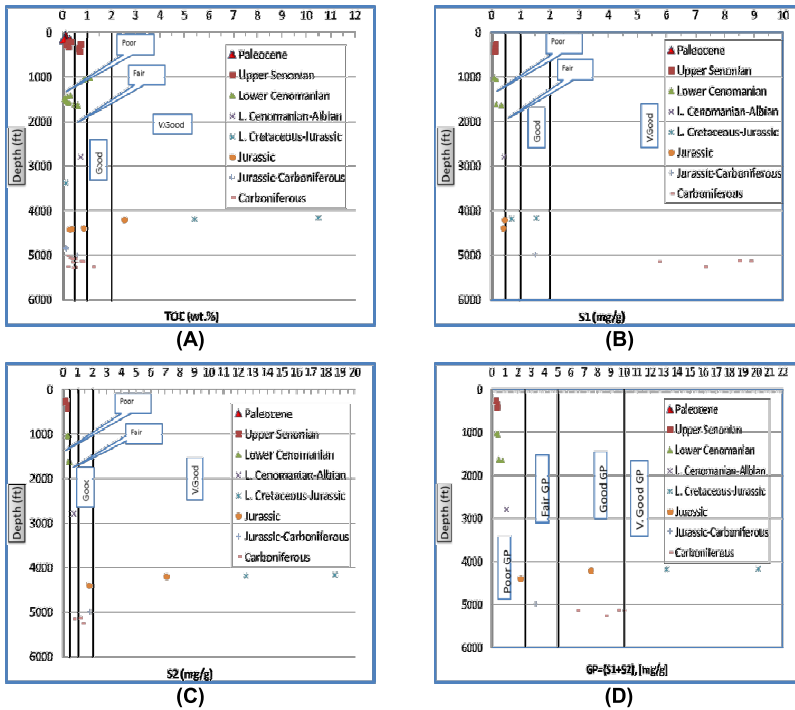


Fig. 29. Geochemical analysis plots of organic matter richness and hydrocarbon generation potential of Ammonite-1 well: (A) Organic carbon richness (TOC), (B) Free hydrocarbons percent (mg HC/g rock), (C) Residual petroleum potential (mg HC/g rock) and (D) Genetic potential (mg/g).

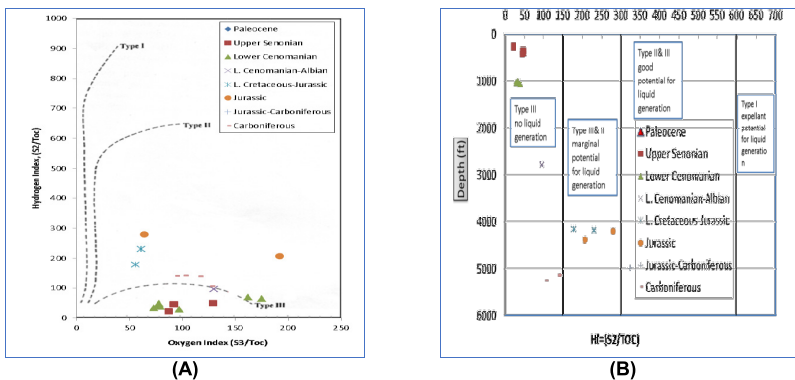


Fig. 30. Geochemical analysis plots of organic matter types of Ammonite-1 well: (A) Modified Van Krevelen type diagram showing kerogen type and (B) Hydrocarbon index.

of 429°C. This indicates the marginal maturity of the organic matter (Fig. 31-A). The use of thermal maturity variation from the HI-Tmax cross-plot (Fig. 31-B) indicates the variation from gas-prone (Type III) kerogen to oil and gas-prone (Type II) kerogen. The thermal maturity is also verified in (Fig. 31-C) which indicates that the samples majority lies in the area of effective non-source rock.

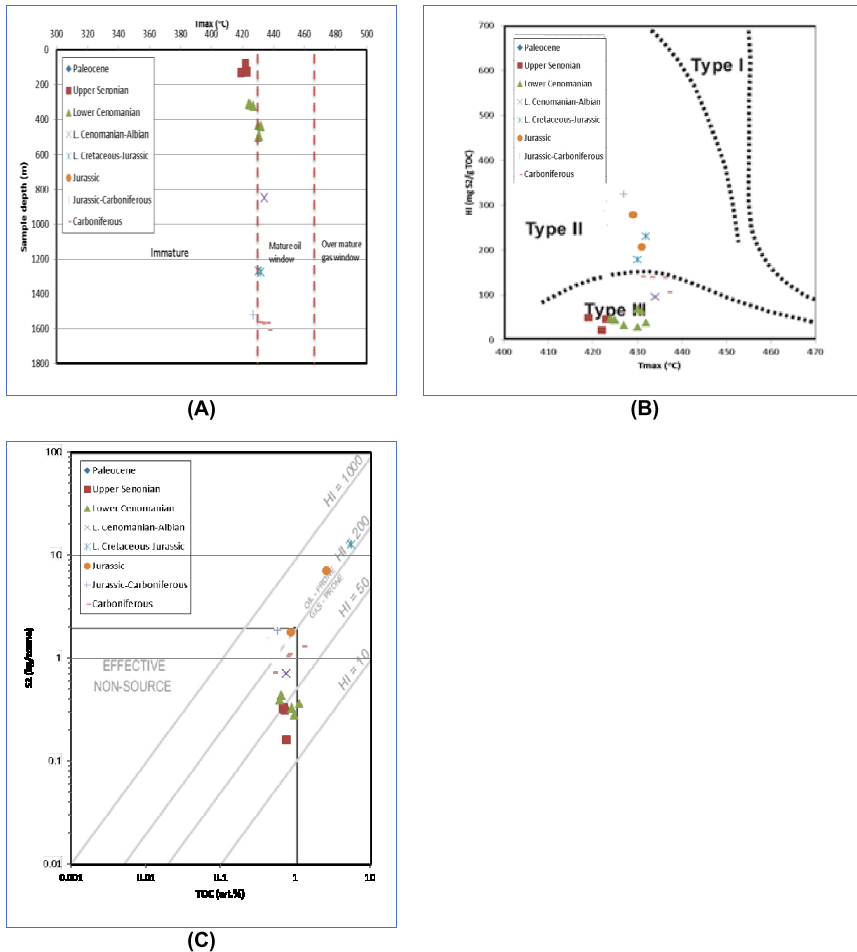


Fig. 31. Geochemical analysis plots of organic matter maturation of Ammonite-1 well: (A) Tmax versus depth, (B) HI-Tmax crossplot (Espitalié, 1986) showing organic matter quality variation and (C) TOC-S2 cross-plot (Langford and Blanc-Valleron, 1990).

6. Conclusions

The comparison of the obtained depth to basement map and the regional Sandwell satellite-derived free-air gravity anomaly map shows that the major basin detected in this study may be a part of a deeper and larger basin extending to the north and northeast, in the Egyptian lands, and to the southwest, in the Libyan lands (Kufra basin). There is a similarity between the Kufra and the area of investigation (West Dakhla and Dakhla) basins in the structure framework and stratigraphic sequence. The thickness of the sedimentary cover looks adequate to support the other elements of the hydrocarbon system.

This study can help in the reconnaissance regional phase for outlining the major basins and sub-basins and delineating the in-between ridge belts. This phase facilitates to enter the exploration phase where the trapping-promising parts can be inferred from the seismic surveying and deep wells penetrating the Silurian section. Gravity and Magnetic data (Residual and basement maps) suggest that there will not be a big challenge to find the traps through more detailed seismic work.

The TOC is varying from a poor to a very good source rock. Poor genetic potential is indicated from the values along the section that is ranging from 0.29 to 20.17 mg/g rocks few are good at the Jurassic and Lower Cretaceous-Jurassic Ages. Thermal maturity is also verified and indicates that the main samples are lying in the area of effective non-source rock.

Acknowledgements. Authors are appreciating and wishing to thank the EGPC and Dana Petroleum Company for permitting the use of data in this study.

Authors' contributions. Conceptualization by Nabih M. and Gawish N. S.; Methodology and investigation by Ghoneimi A., Gawish N. S. and Nabih M.; Writing – original draft preparation by Ghoneimi A. and Nabih M.; Writing – review and editing, Ghoneimi A., Gawish N. S. and Nabih M.; Supervision by Ghoneimi A.; All authors have read and agreed to the published version of the manuscript.

References

- Abrams M. A., Greb M. D., Collister J. W., Thompson M., 2016: Egypt far Western Desert basins petroleum charge system as defined by oil chemistry and unmixing analysis. *Mar. Pet. Geol.*, **77**, 54–74. doi: 10.1016/j.marpetgeo.2016.05.035.
- Afife M., Littke R., Lashin A., Abdel all M. 2017: Geochemistry, generation and maturation of the hydrocarbons at Wadi Al-Rayan oil field, Western Desert of Egypt.

- Pet. Sci. Technol., **35**, 12, 1253–1262, doi: 10.1080/10916466.2017.1321665.
- Bellini E., Massa D., 1980: A stratigraphic contribution to the Paleozoic of the southern basins of Libya. In: Salem M. J., Brusrewil M. T. (Eds.): *The Geology of Libya I*. Elsevier, Amsterdam, 3–56.
- Cheng J. E., 2020: Petroleum System of Shoushan Basin, Western Desert, Egypt. *Geol. Behav. (GBR)*, **4**, 1, 1–8, doi: 10.26480/gbr.01.2020.01.08.
- Craig J., Rizzi C., Said F., Thusu B., Luning S., Asbali A., Keeley M. L., Bell J. F., Durham M. J., Eales M. H., Beswetherick S., Hamblett C., 2008: Structural styles and prospectivity in the Precambrian and Palaeozoic Hydrocarbon systems of North Africa. In: Salem M. J. (Ed.): *The Geology of East Libya*, Gutenberg Press, Malta, 51–122, <http://www.sepmstrata.org/page.aspx?&pageid=148&4>.
- EGPC, 1992: Exploration and production review (part 1), Western Desert, oil and gas fields, (a comprehensive overview). EGPC, Cairo, 431 p.
- El Sherief M. A., Elbastawesy M. A., Abdeldayem A. L., Mohamed S. A., 2020: Source Rock Evaluation of Some Mesozoic and Paleozoic Rocks, Faghur Basin, Neith Field, North Western Desert, Egypt. *Delta J. Sci.*, **42**, 2, 45–57, ISSN: 1012-5965, doi: 10.21608/DJS.2020.139841.
- Espitalié J., 1986: Use of Tmax as a maturation index for different types of organic matter. Comparison with vitrinite reflectance. In: Burrus J. (Ed.): *Thermal Modelling in Sedimentary Basins*. Publications de l'Institut Français du Pétrole/Institut Français du Pétrole, 44, Editions Technip, Paris, 475–496.
- Farooqui M. Y., Farhoud K., Mahmoud D., El-Barkooky A. N., 2012: Petroleum potential of the interpreted Paleozoic geoseismic sequences in the South Diyar Block, Western Desert of Egypt. *GeoArabia*, **17**, 3, 133–176, Gulf PetroLink, Bahrain, doi: 10.2113/geoarabia1703133.
- Gossel W., Ebraheem A. M., Wycisk P., 2004: A very large-scale GIS-based groundwater flow model for the Nubian sandstone aquifer in Eastern Sahara (Egypt, northern Sudan and eastern Libya). *Hydrogeol. J.*, **12**, 6, 698–713, doi: 10.1007/s10040-004-0379-4.
- Hallett D., Clark-Lowes D., 2016: *Petroleum Geology of Libya*, Second Edition, Elsevier, ISBN: 978-0-44463517-4. 391 p.
- Hamimi Z., El-Barkooky A. N., Martínez Frías J., Fritz H., Abd El-Rahman Y. (Eds.), 2020: *The Geology of Egypt*. Regional Geology Reviews, Springer Nature Switzerland, doi: 10.1007/978-3-030-15265-9.
- Hesse K. H., Hissene A., Kheir O., Schnaecker E., Schneider M., Thorweihe U., 1987: Hydrogeological investigations of the Nubian Aquifer System, Eastern Sahara. In: Kilitzsch E., Schranck E. (Eds.): *Research in Egypt and Sudan*, Dietrich Reimer, Berlin, Berl. Geowiss. Abh., (A), **75**, 397–464.
- Hissene A. M., 1986: *Geologie und Hydrogeologie des Erdis-Bekkens, NE-Tschad*. Berl. Geowiss. Abh., (A), **76**, 1–67.
- Hollander D. J., Bessereau G., Belin S., Huc A. Y., Houzay J. P., 1991: Organic matter in the early Torcian shales, Paris Basin, France: a response to environmental changes. *Rev. De 1 Inst. France Petrol.*, **46**, 543–562, <http://www.sepmstrata.org/page.aspx?&pageid=148&4>.

- IRC (Industrial Research Centre and Geol. Research and Minerals Dept., Libya), 1985: Geological Map of Libya 1:1000000, sheet SE, Esselte Maps, Stockholm.
- Kheir O. M., 1986: Hydrogeology of Dongola area, northern Sudan. *Berl. Geowiss. Abh.*, (A), **74**, 1–81.
- Klitzsch E., 1984: Northwestern Sudan and bordering areas; geological developments since Cambrian time. *Berl. Geowiss. Abh.*, (A), 50: 23–45.
- Klitzsch E., 1990: Paleogeographical development and correlation of Continental Strata (former Nubian Sandstone) in northeast Africa. *J. Afr. Earth Sci. Mid. East*, **10**, 1–2, 199–213, doi: 10.1016/0899-5362(90)90055-j.
- Klitzsch E. H., 2000: The structural development of the Murzuq and Kufra basins—significance for oil and mineral exploration (Chapter 7). In: Sola M. A., Worsley D. (Eds.): Geological Exploration in Murzuq Basin, The Geological Conference on Exploration in the Murzuq Basin held in Sabha September 20–22, 1998, 143–150, doi: 10.1016/b978-044450611-5/50009-x.
- Klitzsch E. H., Squyres C. H., 1990: Paleozoic and Mesozoic Geological History of North-eastern Africa Based Upon New Interpretation of Nubian Strata. *Am. Assoc. Pet. Geol. Bull.*, **74**, 8, 1203–1211, doi: 10.1306/0c9b2457-1710-11d7-8645000102c1865d.
- Langford F. F., Blanc-Valleron M.-M., 1990: Interpreting Rock-Eval pyrolysis data using graphs of pyrolyzable hydrocarbons vs. Total Organic Carbon. *Am. Assoc. Pet. Geol. Bull.*, **74**, 6, 799–804, doi: 10.1306/0C9B238F-1710-11D7-8645000102C1865D.
- Lüning S., Craig J., Fitches B., Mayouf J., Busrewil A., El Dieb M., Gammudi A., Loydell D., McIlroy D., 1999: Re-evaluation of the petroleum potential of the Kufra Basin (SE Libya, NE Chad): does the source rock barrier fall? *Mar. Pet. Geol.*, **16**, 7, 693–718, doi: 10.1016/S0264-8172(99)00013-6.
- Lüning S., Craig J., Fitches B., Mayouf J., Busrewil A., El Dieb M., Gammudi A., Loydell D. K., 2000: Petroleum source and reservoir rock re-evaluation in the Kufra Basin (SE Libya, NE Chad, NW Sudan) (Chapter 8). In: Sola M. A., Worsley D. (Eds.): Geological Exploration in Murzuq Basin, The Geological Conference on Exploration in the Murzuq Basin held in Sabha September 20–22, 1998, 151–173, doi: 10.1016/B978-044450611-5/50010-6.
- Meinhold G., Le Heron D. P., Elgadry M., Abutarruma Y., 2015: The search for ‘hot shales’ in the western Kufra Basin, Libya: geochemical and mineralogical characterisation of outcrops, and insights into latest Ordovician climate. *Arab. J. Geosci.*, **9**, 1, doi: 10.1007/s12517-015-2173-0.
- Meinhold G., Whitham A. G., Howard J. P., Stewart J. C., Abutarruma Y., Thusu B., 2013: Hydrocarbon source rock potential of Latest Ordovician – Earliest Silurian Tanezzuft Formation shales from the eastern Kufra Basin, SE Libya. *J. Pet. Geol.*, **36**, 2, 105–115, doi: 10.1111/jpg.12546.
- Meshref W. M., 1990: Tectonic framework. In: Said R., (Ed.): The geology of Egypt. A. A. Blakema, Rotterdam, 113–155.
- Moustafa A. R., Saoudi A., Moubasher A., Ibrahim I. M., Molokhia H., Schwartz B., 2003: Structural setting and tectonic evolution of the Bahariya Depression, Western

- Desert, Egypt. *Gulf PetroLink, Bahrain, GeoArabia*, **8**, 1, 91–124, doi: 10.2113/geoarabia080191.
- Pallas P., 1980: Water Resources of the Socialist People's Libyan Arab Jamahiriya. In: Salem M. J., Busrewil M. T. (Eds.): *The Geology of Libya. Proceedings of the Second Symposium on the Geology of Libya*, Academic Press, London, **2**, 539–594.
- Peters K. E., 1986: Guidelines for evaluating petroleum source rock using programmed pyrolysis. *Am. Assoc. Pet. Geol.*, **70**, 3, 318–329, doi: 10.1306/94885688-1704-11D7-8645000102C1865D.
- Peters K. E., Xia X., Pomerantz A. E., Mullins O. C., 2016: Geochemistry Applied to Evaluation of Unconventional Resources (Chapter 3). In: Zee Ma Y., Holditch S. A. (Eds.): *Unconventional Oil and Gas Resources Handbook (Evaluation and Development)*. Gulf Professional Publishing, 71–126, doi: 10.1016/b978-0-12-802238-2.00003-1.
- Peterson J. A., 1985: *Geology and Petroleum resources of north-central and northeastern Africa*. Open-File Report 85-589, USGS, Dept. of the Interior.
- Reid A. B., Allsop J. M., Granser H., Millett A., Somerton I. W., 1990: Magnetic interpretation in three dimensions using Euler deconvolution. *Geophysics*, **55**, 1, 80–91, doi: 10.1190/1.1442774.
- Said R., 1962: *The geology of Egypt*. Elsevier Publ. Co., Amsterdam Oxford and New York, 377 p.
- Salama M. M., El Ebaidi S. K., 2016: Quality of Water Resources in Kufra Basin, SE Libya. “Science Stays True Here”, *Biol. Chem. Res.*, 391–398, Science Signpost Publishing.
- Sandwell D. T., Garcia E., Soofi K., Wessel P., Smith W. H. F., 2013: Towards 1-mGal accuracy in global marine gravity from CryoSat-2, Envisat, and Jason-1. *Lead. Edge*, **32**, 8, 892–899, doi: 10.1190/tle32080892.1.
- Sandwell D. T., Müller R. D., Smith W. H. F., Garcia E., Francis R., 2014: New global marine gravity model from CryoSat-2 and Jason-1 reveals buried tectonic structure. *Science*, **346**, 6205, 65–67, doi: 10.1126/science.12582.
- Sandwell D. T., Smith W. H. F., 2009: Global marine gravity from retracked Geosat and ERS-1 altimetry: Ridge Segmentation versus spreading rate. *J. Geophys. Res. Solid Earth*, **114**, B1, B01411, doi: 10.1029/2008JB006008.
- Schlumberger, 1984: *Geology of Egypt*. In: Paper presented at the Well Evaluation Conference, Schlumberger, Cairo, 1–64.
- Schlumberger, 1995: *Geology of Egypt*. In: Paper presented at the Well Evaluation Conference, Schlumberger, Cairo, 58–66.
- Schmieder M., Buchner E., Le Heron D. P., 2009: The Jebel Hadid structure (Al Kufrah Basin, SE Libya)—A possible impact structure and potential hydrocarbon trap? *Mar. Pet. Geol.*, **26**, 3, 310–318, doi: 10.1016/j.marpetgeo.2008.04.003.
- Seber D., Vallvé M., Sandvol E., Steer D., Barazangi M., 1997: Middle East Tectonics: Application of geographic Information Systems (GIS). *Geol. Soc. Amer. Today*, **7**, 2, 1–5.

- Sefelnasr A. M., 2007: Development of groundwater flow model for water resources management in the development areas of the Western Desert, Egypt. Thesis, The Faculty of Natural Sciences III of the Martin Luther University Halle-Wittenberg in partial fulfilment of the requirements for the award of the degree of Doctor of Natural Sciences.
- Taha M. A., 1992: Mesozoic rift basins in Egypt, their southern extension and impact on future exploration. In: Proceedings of the 11th Petroleum Exploration and Production Conference, Cairo, 1992. The Egyptian General Petroleum Corporation, **2**, 1–19.
- Thorweihe U., Heintz M., 2002: Groundwater resources of the Nubian Aquifer System, NE-Africa. Modified synthesis submitted to: Observatoire du Sahara et du Sahel. OSS, Paris, 23 p., available at http://reseau-tchad.org/cdig/media/SIRE_Biblio/Publications/Hydrogeologie/Groundwater_resources_NSAS_2002_Thorweihe.pdf.